Cooperative deformation of hydrogen bonds in beta-strands and beta-sheet nanocrystals

Zhao Qin and Markus J. Buehler*

Laboratory for Atomistic and Molecular Mechanics, Department of Civil and Environmental Engineering, Massachusetts Institute of Technology, 77 Massachusetts Avenue, Room 1-235A&B, Cambridge, Massachusetts 02139, USA

(Received 24 August 2010; revised manuscript received 22 October 2010; published 14 December 2010)

Beta-sheet protein domains are stabilized by weak hydrogen bonds, yet materials such as silk—whose ultimate tensile strength is controlled primarily by this secondary structure—can exceed the ultimate tensile strength of steel. Earlier work has suggested that this is because hydrogen bonds deform cooperatively within small protein domains to reach the maximum strength. Here we study the atomistic mechanism of this concerted deformation mechanism by applying an elastic structural model, used to solve the deformation field of the chemical bonds in beta-sheet nanostructures under stretching and thereby identify the number of hydrogen bonds that deform cooperatively. Through this analysis, we predict the optimal beta-strand and beta-sheet nanocrystal size associated with reaching the maximum usage of hydrogen bonds under loading applied per unit material volume. Our results, albeit based on a simple model and analytical equations, quantitatively agree with results based on experimental and molecular-dynamics studies and provide physical insight into the underlying molecular mechanisms of weak bond cooperativity. A comparison with the size of hydrogen bond clusters in biology reveals excellent agreement with the cluster sizes predicted by our analysis, suggesting that perhaps the confinement of hydrogen bonds into nanoscale elements is a universal biological design paradigm that turns weakness to strength. The parameters used in this study could be modified and applied to other protein and polymer structures, which imply potential applications of our model in understanding the physics of deformation and failure in a broader range of biological and polymer materials, as well as in *de novo* biomaterial design.

DOI: 10.1103/PhysRevE.82.061906 PACS number(s): 87.15.La, 62.25.−g, 82.37.Rs, 62.20.F−

I. INTRODUCTION

The use of silk by humans is an ancient practice, where silkworm silk has been in use since more than 5000 years in China. At that time, people used silk woven into luxurious cloth and paper because they are light, transparent, and can last for a long time. More recently, additional intriguing properties of silk were revealed by research and related applications for its broad use as engineering material have been pursued [1–3]. For example, silk is used as tissue scaffold in facilitating wound healing or tissue regeneration because it is biocompatible and degradable in biological environments [2,4]. Moreover, in the past decades researchers discovered that some types of spider silk have a remarkable ultimate tensile strength greater than steel, and since then much effort has been expended on spider silk research with the long-term goal to understand its structure as well as to develop application in industrial and military fields [5,6].

Silk is composed of beta-sheet nanocrystals mingled with less orderly helix and beta-turn structures that form a semiamorphous domain [7–9]. In this structure, beta-sheet nanocrystals connect multiple chains that embedded in semiamorphous domains. It has been suggested that the semiamorphous domain makes the material soft and flexible at the relaxed state [7,8,10]. Under extreme loading conditions, peptide chains in the semiamorphous domain rotate to align with the force direction, and the strength of the material is ultimately defined by the maximum force that can be sustained by hydrogen-bonded beta-sheet nanocrystals [10–15]. A recent study used computational simulations to reveal that the beta-sheet nanocrystal size is important in defining the ultimate tensile force of these nanocrystals, which is enhanced by the cooperative deformation of hydrogen bonds (H bonds) and the interplay of shearing versus bending deformation as a function of nanocrystal size [14] where it was suggested that the cooperative behavior of H bonds in clusters may explain how silks and other H-bond rich protein materials can reach extreme levels of strength in spite of weak bonding. In another investigation of the alpha-beta transition in coiled-coil protein filaments it was demonstrated that this process is also related to cooperative deformation and failure mechanism of H bonds and that this process is size dependent as well [16], suggesting that size effects are crucial for our understanding of key properties in a variety of protein materials. In the study reported here, we focus on the shearing deformation of H bonds within beta-strands and beta-sheet nanocrystals as shown in Figs. 1(a) and 1(c), respectively. By using an elastic structural model, we solve for the deformation field of H bonds within the beta-sheet nanocrystal and identify the size of the cooperative H-bond region under mechanical loading.

II. MATERIALS AND METHODS

We provide an overview of the model and calculation method used here. In Sec. II A we introduce the geometry of the elastic structural model, in Sec. II B we describe how we calculate the deformation field as well as the characteristic length of the model, and in Secs. II C and II D we present the details of the computational procedure utilized to obtain the

*Corresponding author; mbuehler@mit.edu

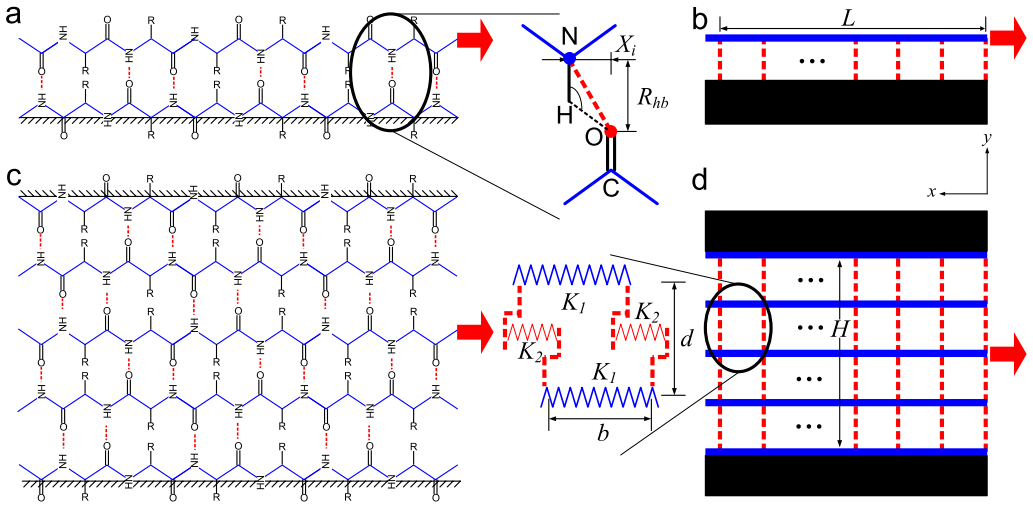

FIG. 1. (Color online) The geometry, boundary condition, and coordinate system of the atomic model and calculation model used in this study. Panel (a): atomic model and boundary conditions of single beta strand consisting of two antiparallel peptide chains and a series of H bonds between them. One chain is fixed while the other chain end is stretched in $-x$ direction by an applied force F_{app}. Panel (b): model geometry corresponding to the atomistic model in panel (a). The structure is composed of backbone elements and H-bond elements and has a total length L. Panel (c): atomistic model and boundary conditions of the beta-sheet nanocrystal. The structure is composed of multiple peptide chains and stabilized by H bond between each of the layers. The layers at the top and bottom are fixed, while the middle one is stretched in the $-x$ direction by an applied force F_{app}. Panel (d): model geometry corresponding to the atomistic model depicted in panel (c). The structure has a total length L and thickness H.

stiffness parameters of the H bond and backbone in our model, respectively.

A. Beta-strand and beta-sheet nanocrystal model

The beta-strand model includes two peptides in the antiparallel form, and the beta-sheet nanocrystal includes multiple peptides with beta strands arranged in an antiparallel form, as shown in Figs. 1(a) and 1(c). The length of the model is given by L and the thickness is H. For the beta-strand model as shown in Fig. 1(a), one peptide is fixed and the other one is stretched by a tensile force F_{app}. For the beta-sheet nanocrystal model as shown in Fig. 1(c), we fix the top and bottom layers and apply the stretching force to the middle layer. The force application point is defined as zero point of the coordinate system, and coordinate directions are depicted in Fig. 1. The deformation of each H bond is measured by the displacement difference between the donor and the acceptor. The average distance between two neighborhood H bonds is given by b in the x direction and d in the y direction. Earlier work has shown that the strength of beta-sheet nanocrystals controls the ultimate strength of silks, owing to the fact that the nanocomposite found in silk consists of a combination of relatively soft semiamorphous domains and more rigid and beta-sheet nanocrystals [15]. As demonstrated in a recent study [15] the arrangement of these two constituents in silk can be approximated as a serial combination of semiamorphous domains and beta-sheet nanocrystals. The setup used here provides a simple model system to focus solely on the strength properties of beta-sheet nanocrystals. It is noted that future work could focus on the development of models that incorporate both semiamorphous domains and beta-sheet nanocrystals.

B. Elastic structural model

In this section we explain the elastic structural model applied here to obtain the deformation field within the bonds of the beta-sheet models. We start with a beta-strand model and then extend the method to the beta-sheet nanocrystal. The beta-strand model contains N H bonds (where $N=L/b+1$), as shown in Fig. 1(b), and is made up of two elements: the polypeptide backbone and H bonds. We model them as truss elements connected by nodes and use harmonic springs to describe their tension and compression properties. Each node represents an amino acid connected to an H bond. The stiffness of the backbone element is given by K_1 and the stiffness of the H-bond element in the shearing direction is K_2. The displacement X_j for each amino acid j under stretching can be solved by

$$K_{ij}X_j = F_i, \tag{1}$$

where F_i is the force applied at each amino acid. We pull the center strand with a force of $F_1=-F_{app}$ and $F_i=0(i\neq 1)$. The parameter K_{ij} denotes the stiffness matrix, which is established by assembling the stiffness of each amino acid. Each component of the stiffness matrix is given by

$$K_{ij} = \begin{cases} K_1 + K_2 & \text{for } i = j = 1, N \\ 2K_1 + K_2 & \text{for } i = j \in [2, N-1] \\ -K_1 & \text{for } |i-j| = 1 \\ 0 & \text{otherwise.} \end{cases} \tag{2}$$

For example, the stiffness matrix of the model shown in Fig. 1(a) is found to be

$$\bar{K} = \begin{bmatrix} K_1+K_2 & -K_1 & 0 & \cdots \\ -K_1 & 2K_1+K_2 & -K_1 & \cdots \\ \cdot & \cdot & \cdot & 0 \\ 0 & \cdot & \cdot & \cdot \\ & -K_1 & K_1+K_2 & \end{bmatrix}_{N\times N}. \quad (3)$$

By solving Eq. (1) with K_{ij} given in Eq. (2) and F_i we can find the displacement of each node, X_j. It is noted that in this elastic model X_j is proportional to the applied force F_{app}. Since the lower boundary of the beta strand is fixed, the deformation of each H bond is given by $\Delta x_j = 0 - X_j = -X_j$.

The beta-sheet nanocrystal model, as shown in Fig. 1(d), is an extension of the beta-strand model into the y direction. It features N parallel H bonds and M layers (where $N = L/b + 1$ and $M = H/d + 1$). The force vector is given by $F_f = -F_{applied}$ and $F_i = 0 (i \neq f)$, where f is the node number with the applied force. We consider this force boundary condition of lateral loading for the beta-sheet nanocrystal because of the geometric character found in spider silk. The beta-sheet nanocrystals in silk are embedded in a semiamorphous matrix (composed of helical and coiled domains, e.g., 3_1 helices), where discrete strands are connected to the amorphous matrix. Under mechanical loading, the amorphous region unwinds first and, subsequently, lateral loading is applied to the beta-sheet nanocrystal [15]. To study the cooperative deformation of H bonds in this system, we apply a force at the middle strand, change the nanocrystal size, and study the deformation field of H bonds of each size. The stiffness matrix of the structure is given by

$$K_{ij} = \begin{cases} \infty & \text{for } i = j \in [1,N] \\ K_1 + 2K_2 & \text{for } i = j = aN+1,\ i = j = (a+1)N-1,\ a \in [1,M-2] \\ 2(K_1+K_2) & \text{for } i = j \in [aN+2,(a+1)N-2],\ a \in [1,M-2] \\ -K_1 & \text{for } |i-j| = 1,\ i \in [aN+1,(a+1)N],\ j \in [aN+2,(a+1)N-1],\ a \in [1,M-2] \\ -K_2 & \text{for } |i-j| = N,\ i \in [N+1,(M-1)N],\ j \in [2N+1,(M-2)N] \\ \infty & \text{for } i = j \in [MN-N,MN] \\ 0 & \text{otherwise}, \end{cases} \quad (4)$$

which includes the fixed boundary conditions at the top and bottom layers. For example, the stiffness matrix of the model shown in Fig. 1(c) is found to be

$$\bar{K} = \begin{bmatrix} \begin{bmatrix} \infty & & \\ 0 & \cdots & 0 \\ & & \infty \end{bmatrix}_{N\times N} & 0 & 0 \\ 0 & \begin{bmatrix} K_1+2K_2 & -K_1 & 0\cdots & -K_2\cdots \\ -K_1 & 2(K_1+K_2) & -K_1 0\cdots & -K_2\cdots \\ & \cdots & & 0 \\ 0 & & \cdots & \\ & -K_2\cdots 0 & -K_1 & K_1+2K_2 \end{bmatrix}_{(M-2)N\times(M-2)N} & 0 \\ 0 & 0 & \begin{bmatrix} \infty & & \\ 0 & \cdots & 0 \\ & & \infty \end{bmatrix}_{N\times N} \end{bmatrix}_{MN\times MN}. \quad (5)$$

Similar as in the beta-strand case, by solving Eq. (1) we obtain the displacement of each node X_j. The deformation of each H bond is the difference of the displacements of the two nodes connected by this H bond, and it is given by $\Delta x_j = |X_j - X_{j+N}|$. It is noted since we focus on shearing deformation of the beta-sheet nanocrystals; we assume each node in this model has only one degree of freedom in the x direction. This assumption is based on the observation that beta-strand and short beta-sheet nanocrystal structures are usually observed in spider silks and that the shear stress is dominant to cause the deformation of hydrogen bonds, which leads to structure failure under the stretching loading as observed in earlier simulations [14]. Moreover, we focus on the deformation character of the crystal before the rupture of H bonds, and in such a case, the movement of strands perpendicular to the in-plane direction is rather small compared with that in the loading direction.

We obtain the deformation of each H bond via the elastic model shown above and we observe that the H bond nearest to the applied force has the maximum deformation, where

the deformation decays quickly as the node is located further away from the loading point. This is because the backbone is not rigid, and thus the deformation is not uniform but decreases in the direction opposite to the applied force. This phenomenon of decaying displacements can be described by an exponential decay equation $d\Delta x/dx \sim -\Delta x$ since the elastic deformation of the backbone depends on the applied force. By solving this equation we obtain

$$\Delta x = Ae^{-x/x_0}, \tag{6}$$

where A is the deformation of the first H bond close to the force point (proportional to the applied force F_{app}), x is the coordinate of the bond as defined in Fig. 1, and x_0 denotes the rate of decay of the function. This type of function is widely used to study how one quantity decreases with respect to an increasing scalar [17]. Following this approach we define x_0 as a characteristic length scale, emphasizing that it is independent of the applied force value F_{app} (only A is influenced by the level of applied force F_{app} and proportional to it). For our specific case x_0 defines a characteristic length scale associated with the number of H bond that deforms more significantly and more uniformly, and therefore the length is adopted to define the size of the cooperative deformation of H bonds. We therefore use Eq. (6) to fit the deformation of H bonds along the x and $\pm y$ directions and use x_0 to identify the size of the cooperative deformation of the beta-strand and the beta-sheet nanocrystals under stretching (where a larger value of x_0 means more H bonds near the force point deform uniformly). We normalize the length and coordinate parameters in the x and y directions by b and d, respectively, so that the results are given in the unit of number of H bonds.

C. Stiffness of H bonds

In this section we explain how the parameter K_2, the shearing stiffness of H bonds, is obtained directly from the interatomic potential. The calculation is based on the Dreiding force field model [18], in which the H-bond energy is given by

$$E_{hb} = D_{hb}[5(R_{hb}/R_{DA})^{12} - 6(R_{hb}/R_{DA})^{10}]\cos^4(\theta_{DHA}), \tag{7}$$

where D_{hb} has the physical meaning as the depth of the H-bond energy and R_{hb} as the zero force distance for the H bond if $\cos(\theta_{DHA})$ keeps constant, and those two are parameters from Dreiding model for the H bond. The parameter R_{DA} is the distance between the donor (N here) and the acceptor (O here), and θ_{DHA} is the angle for $\angle NHO$ as shown in Fig. 1(a). The reason to choose the Dreiding force field to describe the force-extension behavior of hydrogen bonds is that it provides an explicit expression of the hydrogen bond energy, including angular terms. By using this expression, we are able to obtain an explicit expression of the elastic stiffness of the H bond. Since the length of the covalent bond N-H is a_1 in the Dreiding force field, by taking the average distance between two neighboring beta strands as a constant, the geometric variants in Eq. (7) can be expressed as

$$R_{DA} = \sqrt{x^2 + R_{hb}^2}, \tag{8}$$

TABLE I. Parameters for the elastic structural model used in calculations.

K_1=4153 pN/Å
K_2=843 pN/Å
k_{SMD}=10 kcal/mol Å^{-2}
D_{hb}=9.5 kcal/mol
ϕ=180°
ψ=180°
R_{hb}=2.75 Å
a_1=0.98 Å
d=4 Å
b=3.5 Å

$$\cos(\theta_{DHA}) = -\frac{R_{hb} - a_1}{\sqrt{[x^2 + (R_{hb} - a_1)^2]}}, \tag{9}$$

where x is the shearing displacement of the donor relative to the acceptor. The parameter values are summarized in Table I for an overview.

With numerical values of all parameters determined, we can now solve the reaction force for a single H bond within a beta-strand structure under shearing as

$$F = \frac{\partial E_{hb}}{\partial x} = D_{hb}\left[60\left(-\frac{R_{hb}^{12}}{R_{DA}^{13}} + \frac{R_{hb}^{10}}{R_{DA}^{11}}\right)\frac{dR_{DA}}{dx}\cos^4(\theta_{DHA}) - \left(5\frac{R_{hb}^{12}}{R_{DA}^{12}} - 6\frac{R_{hb}^{10}}{R_{DA}^{10}}\right)\frac{4x(R_{hb} - a_1)^4}{[x^2 + (R_{hb} - a_1)^2]^3}\right] \tag{10}$$

and the elastic stiffness of each H bond as

$$K_2 = \left.\frac{\partial F}{\partial x}\right|_{x=0} = \frac{4D_{hb}}{(R_{hb} - a_1)^2}. \tag{11}$$

Here we derive the linear elastic modulus of the H bond, which is based on its response upon shear loading around equilibrium state (x=0). Without this assumption, it is true that the tangent modulus is nonlinear with its elongation in x direction; however, this effect is small before rupture. Moreover, in our studies the maximum deformation of a single H bond is 0.64 Å before rupture; the force obtained from the full-potential model [Eq. (10)] is less than 15% smaller than in the linear case.

D. Stiffness of polypeptide backbone

In this section we show how to derive the parameter K_1 as the stiffness of the polypeptide backbone. This parameter refers to the stiffness of a polyalanine chain with a unit length b that equals the average distance between two neighborhood H bonds in the x direction. A polyalanine chain of 14 amino acids is modeled in the CHARMM19 force field and by using the CHARMM code [19]. The reason why we use this kind of simple peptide model is twofold. First, alanine is a major component of the spider silk beta-sheet nanocrystal domain. Second, the structure of alanine amino acid is relatively simple, making it easier to study the backbone stiff-

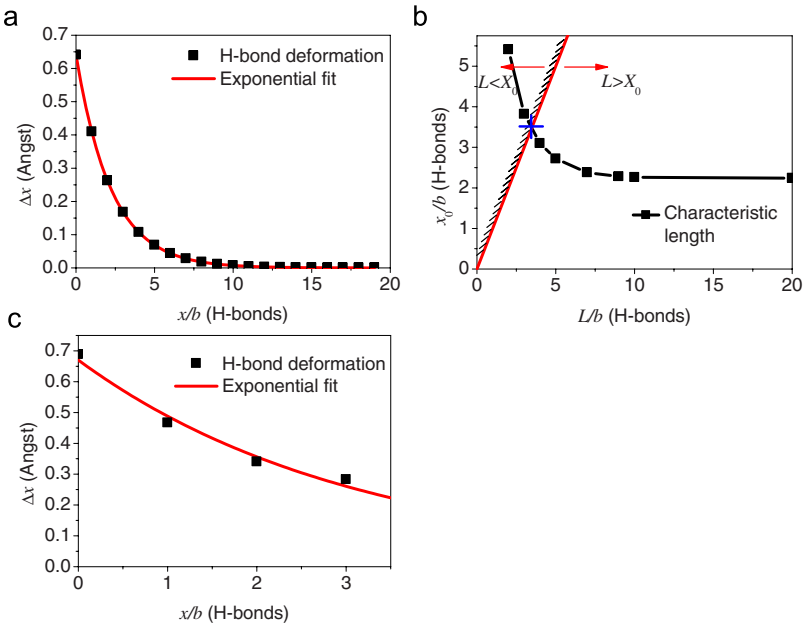

FIG. 2. (Color online) The deformation and characteristic length of each H bond in the beta strand. Panel (a): the deformation of each H bond within a beta strand with a total length $L=20$ H bonds, as well as the exponential fit with a function of $\Delta x=0.64\exp[-x/(2.24b)]$ Å (displacements shown here for $F_{app}=1500$ pN). Panel (b): characteristic length x_0 as a function of the total length L, here the straight line has a function of $x_0=L$, and the region to the right of this line has a physical meaning that the total length of the beta strand must be longer than the characteristic length. The crossing point, as noted, gives the maximum accessible characteristic length $x_{cr}=3.5$ H bonds. Panel (c): the deformation of each H bond within a beta strand with a total length $L=4$ H bonds, as well as the exponential fit with a function of $\Delta x=0.67\exp[-x/(3.10b)]$ Å.

ness without side-chain effects. It is noted that we are cognizant of the fact that hydrophobic and charged side chains can decrease the stiffness by repulsion to each other, while polar side chains can increase the stiffness by forming H bonds between the two of them [20]. The effect of the side chain is neglected here because compared to the backbone, those interactions are much weaker. (The bond energy of H bond is less than 12% of the covalent bond, and other nonbonded interactions are even weaker [18]; the only exception are disulfide bridges between two cysteine side chains. This interaction is strong, but since there is typically only very little (<0.1%) cysteine amino acid in spider silk [21], we neglect this interaction.) The chain starts in a straight conformation, which means the dihedral angles of the peptide structure are $\phi=180°$ and $\psi=180°$. This molecular configuration is selected because it is the same as that of each strand within the beta-sheet structure [20]. We obtain the stiffness of the chain by stretching simulation in the EEF1 solvent model [22,23] at 300 K through the *NVT* ensemble (using the Nose-Hoover thermostat with 1 fs time step) via steered molecular dynamics (SMD) [24]. Boundary conditions consist of a fixed alpha-carbon atom on one chain terminal with an SMD spring constant $k_{SMD}=10$ kcal/mol Å^{-2} and a displacement rate of 0.001 Å/ps at the other end. We measure the slope of the force extension and multiply it by 14 to obtain the proper elastic stiffness of a unit length backbone as K_1. Its value is rate insensitive because it is governed by the elastic property of covalent bonds only, without any bond rupture events or solvent effects. It is noted that our model is similar to elastic network models proposed for protein structures but here developed specifically to capture the elastic details associated with H bonds and the backbone connections [25].

III. RESULTS AND DISCUSSION

We begin our study with investigating a beta-strand model of 20 amino acid length, where the deformation of each H bond as a function of the bond position is shown in Fig. 2(a). We observe that the deformation of the first H bond reaches a maximum value and the deformation of the other H bonds in the system approaches zero relatively fast as the bond coordinate x gets larger. Following the approach outlined in Sec. II we use Eq. (6) to fit the deformation of H bonds as shown in Fig. 2(a) and obtain a deformation function $\Delta x=0.64\exp[-x/(2.24b)]$ Å, which reveals a characteristic number of 2.24 H bonds (note that $A=0.64$ Å for $F_{app}=1500$ pN and that it scales linearly with variations in the applied force, and thereby the resulting x_0 is independent of the choice of F_{app}). This force level of 1500 pN is chosen here because the same force is found in unfolding simulations for beta sheet before rupture, with a constant pull speed of 0.01 Å/ps [26,27].

To investigate the effect of the beta-strand length L on the characteristic length x_0, we change the beta strand to different lengths L and fit each deformation profile to Eq. (6) for each length considered. For each length, the characteristic number of H bonds is summarized in Table II and plotted in Fig. 2(b). It can be observed that this length decreases and converges to 2.24 H bonds as L increases. It is noted that for short $L<4$ (corresponding to the first two columns in Table II), the characteristic length is greater than the strand length, which means that all H bonds within the strand have similar deformations [$\Delta x_i>0.37\Delta x_1$ as shown in Fig. 2(c)]. Since the characteristic length must be shorter than the entire beta-sheet structure, the characteristic length has an effective maximum value of 3.5 H bonds as shown directly in Fig.

TABLE II. Characteristic length x_0 of beta strands with different length L.

L/b (H bonds)	2	3	4	5	7	9	10	20	35	50
x_0/b (H bonds)	5.41	3.82	3.10	2.72	2.38	2.28	2.26	2.24	2.24	2.24

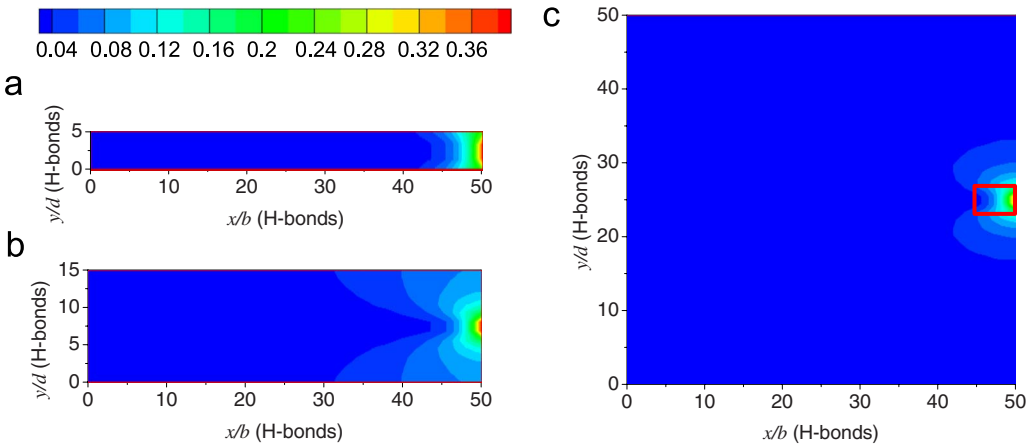

FIG. 3. (Color online) The deformation field of beta-sheet nanocrystal models as illustrated in Fig. 1(d) (displacements shown in the color legend are in Å and obtained for $F_{app}=1500$ pN; note that the resulting x_0 and y_0 are independent of the choice of F_{app}). The deformation of each H bond is given by the color defined in the color bar. The beta-sheet nanocrystal has a dimension of $L\times H$ as in panel (a)—50 $\times$5 H bonds, panel (b)—50$\times$15 H bonds, and panel (c)—50$\times$50 H bonds. The rectangular region indicates an estimate of the extension of the cooperative deformation.

2(b). This means that a structure of 3.5 (or 4 due to their discrete nature) H bonds features the maximum accessible characteristic length and, as such, the maximum ultimate tensile force per unit length (which relates to the shear stress between strands). This result agrees remarkably well with earlier studies done using molecular-dynamics simulations, which showed that a beta-strand length of 3–4 H-bond clusters gives an upper limit of the shear stress [28].

We now extend our study to a beta-sheet nanocrystal model as shown in Fig. 1(d), with a crystal size of L in length and H in width. Figure 3 depicts the deformation field of H bonds within different crystals. We note that the deformation for the H bonds within each single layer (that is, for y =const) decreases in a different fashion. Layers further away from the force application point have a larger characteristic length but a much smaller deformation of the first bond at which the load is applied. For instance, for the model of the nanocrystal featuring 50$\times$50 H bonds as shown in Fig. 3(c), $x_0=1.8$ H bonds at $y=0$, while $x_0=7.8$ H bonds at $y=3$. We compare the deformation profiles along the x (with $y=0$) and y (with $x=0$) directions of beta-sheet nanocrystals of different sizes, and these deformation profiles of the 50$\times$50 H-bond models are shown in Fig. 4. We find that the deformation reaches a maximum value at the force point and decreases along the x and $\pm y$ directions to zero in an exponential fashion. The characteristic lengths in the x and $+y$ directions (noting that the deformation in the $-y$ direction is symmetric) are $x_0=1.8$ H bonds and $y_0=1.32$ H bonds, respectively. These characteristic lengths enable us to estimate the shape of the cooperative deformation as indicated by the rectangular region shown in Fig. 3(c).

We now change the beta-sheet nanocrystal size in both x and y directions and calculate the deformation field for each case the same type of under point loading applied and estimate the characteristic lengths in x and $+y$ directions. The results are summarized in Figs. 5(a) and 5(b). The results reveal that thicker beta-sheet nanocrystals with more layers in the y direction have a slightly smaller x_0, but this effect is

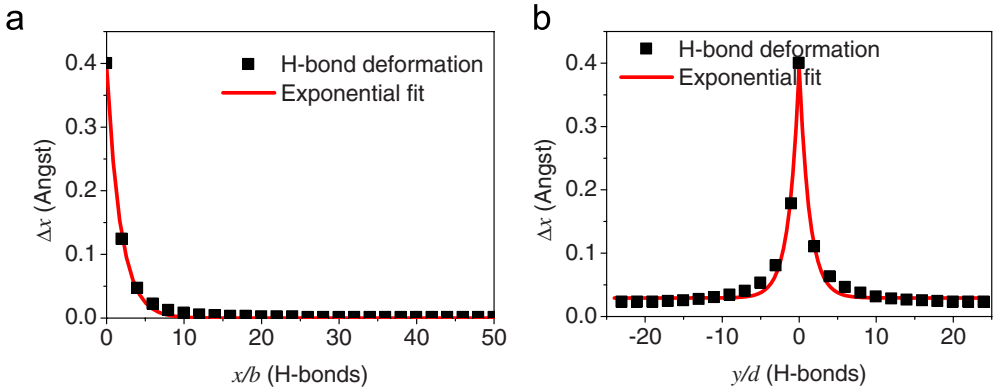

FIG. 4. (Color online) The deformation profiles of the beta-sheet nanocrystal model shown in Fig. 3(c) along the x and y directions, with the force application point defined as the coordinate system's origin. Panel (a): deformation of each H bond along the middle line $y=0$, as well as the exponential fit with a function of $\Delta x=0.4\exp[-x/(1.8b)]$ Å (displacements for all cases shown here obtained for F_{app} =1500 pN). Panel (b): deformation of each H bond along the vertical line $x=0$, as well as the exponential fit with a function of Δx $=0.4\exp[\mp y/(1.32d)]$ Å.

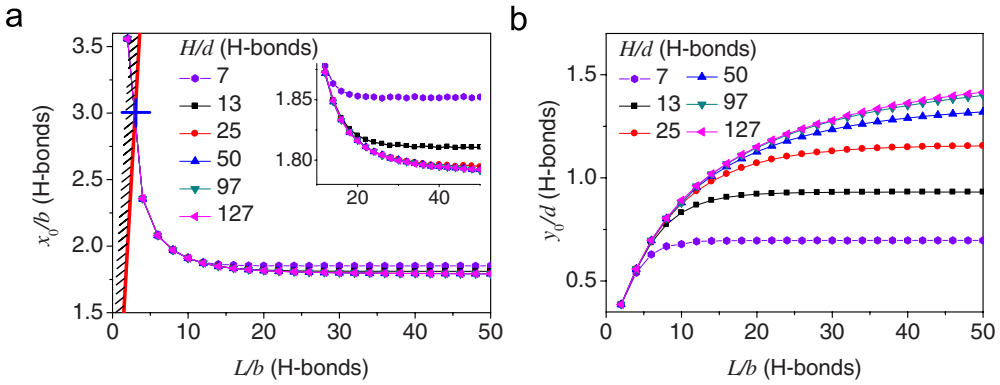

FIG. 5. (Color online) Characteristic lengths in the x and $+y$ directions of beta-sheet nanocrystals of different length L and thickness H. Panel (a): characteristic length x_0 as a function of L and H, here the straight line has a function of $x_0=L$, and the region to the right of this line has a physical meaning that the total length must be longer than the characteristic length. The crossing point, as noted, gives the maximum accessible characteristic length $x_{cr}=3$ H bonds. Panel (b): characteristic length y_0 as a function of L and H.

rather weak and we can only see the difference by considering the detailed view shown in the inset of Fig. 5(a). All beta-sheet nanocrystals of different thickness have a same critical length $x_{cr}=3$ H bonds as the maximum accessible characteristic length as shown in Fig. 5(a). This result is slightly smaller than that of the beta strand because the beta-sheet nanocrystal is fixed at both bottom and top layers, but the beta strand is only fixed at one layer. Most beta-sheet nanocrystals have a characteristic length $y_0=0.5-1.5$ H bonds, as shown in Fig. 5(b), which means that the shearing deformation only concentrates in the central 2 or 4 H-bond layers. This behavior agrees with the phenomenon found in the earlier molecular-dynamics simulations that the point force results in the rupture of only two layers of H-bonded beta strands that make up the beta-sheet nanocrystal and that subsequently creates the characteristic stick-slip motion during failure [14]. The result shown in Fig. 5(b) predicts that by increasing the number of layers, more layers of H bonds deform cooperatively, which should result in rupture events associated with more than two layers of H-bonded beta strands. Moreover, from Fig. 5(b) we also recognize that the relation $y_0=H$ cannot be satisfied when $H>2$ since y_0 is smaller than H. Therefore, we have $y_{cr}=2$ H bonds to meet the condition $y_0=H$ and to make maximum usage of H bonds in the y direction at failure. It is noted that although the result is based on the loading at the center of the beta-sheet nanocrystal the results should be generally valid for loading at other locations in particular since deformation tends to be focused on about two layers. We compare our results for beta-strands and beta-sheet nanocrystals with earlier results obtained by experiment and molecular-dynamics simulation as summarized in Table III [14,28–30]. For beta strands, a statistical study has focused on the analysis of strand lengths of a wide range of beta-sheet structures, and it was found that most structures have strand lengths distributed within the range of 5.4 ± 2.8 H bonds [30]. Earlier molecular-dynamics simulation study suggested a beta-strand length of 3–4 H bonds at which the maximum stress of the beta strand is attained [28]. Our result gives $x_{cr}=3.5$ H bonds, which agrees with those observations. For beta-sheet nanocrystals, it is suggested by experiment that poly-Ala and poly-(Gly-Ala) repeat typically span 4–12 amino acids in nanocrystal of spider silk, which corresponds to 4–12 H bonds as the nanocrystal size [29]. Earlier molecular-dynamics studies investigated the ultimate tensile force of different beta-sheet crystals and suggested that nanocrystals of 2.8–5.7 H bonds in length (in the x direction) and 5–10 H bonds in the thickness (y direction) result in the maximum stress [14]. Our result gives $x_{cr}=3$ H bonds, which agrees with those observations but results in $y_{cr}=2$ H bonds, which is smaller than the earlier findings and thus requires additional discussion. The reason why y_{cr} is different from the earlier results is twofold. Most importantly, in the model reported here we only consider shearing effects but no bending. As it was

TABLE III. Size of the region of cooperative deformation in beta strands and beta-sheet nanocrystals as obtained by theoretical calculation in this study, molecular-dynamics simulation, and experimental methods.

	Beta strand	Beta-sheet crystal	
Approach	x_{cr} (H bonds)	x_{cr} (H bonds)	y_{cr} (H bonds)
Elastic structural model (this study)	3.5	3	2[a]
Molecular simulation [14,28]	3–4	2.8–5.7	5–10 (1–2[b])
Experiment [14,29,30]	2.6–8.2	4–12	4–12

[a]Analysis solely based on shear, without bending.
[b]Failure mode observed in the case of shear dominated deformation shows breaking of 1–2 beta strands out of a beta-sheet nanocrystal.

shown in the detailed analysis reported in [14], if the crystal thickness is significantly larger than its length, bending effects dominate deformation and make the structure weaker as the thickness increases as the deformation field inside the beta-sheet nanocrystal becomes increasingly heterogeneous; however, this effect is not captured in our model since it is only valid for geometries in which shearing dominates. Interestingly, the prediction from our analysis that failure under shear should occur in a few layers only agrees with the atomistic modeling reported in earlier simulation studies of beta-sheet nanocrystals in both silk and amyloid crystals [14,31]. Second, the H-bond stiffness is not constant for different beta-sheet nanocrystals. Earlier density-functional theory calculation results suggested that the adhesion energy for adding a layer to a crystal increases with increasing crystal size, which may imply that the H bond becomes stiffer for beta-sheet nanocrystals with more layers [32].

Our model can be used to estimate the ultimate tensile stress that a beta-sheet nanocrystal can withstand. This serves as an approximation of silk strength, in general, since the strength of beta-sheet nanocrystals controls the ultimate strength of silk as demonstrated in [15]. Using the model that $H=4d$ and $L=7b$ (corresponding to $H=1.87$ nm and $L=2.5$ nm as in [14]), we estimate the deformation function of the middle chain as $\Delta x_i=\Delta x_1 \exp[-x/(2.08b)]$ [as obtained from Eq. (6), as shown in Fig. 5(a)]. Therefore, the ultimate tensile force of the beta-sheet nanocrystal can be estimated to be $F_{ult}=\Sigma_{x=0}^{6b} 2F_{HB}e^{-x/(2.08b)}=2732$ pN since $F_{HB}=AK_2=540$ pN is the average strength of a single H bond [note that $A=0.64$ Å for $F_{app}=1500$ pN before rupture as shown in Fig. 2(a)]. Taking into account that the linear assumption overestimated the force by 15% and also at a factor of 6 by comparing to the experimental rates [14,26,27], the ultimate tensile force of this spider silk crystal would be 387 pN and the corresponding shear strength is 806 MPa. We note that the strength value of 387 pN estimated here agrees with atomic force microscopy experimental results of beta-sheet proteins and estimates based on molecular simulation, which resulted in estimates in the range of 250–400 pN [14,33]. For comparison, in stainless steel (e.g., ASTM A992) the ultimate tensile stress is given by 450 MPa [34] and as such slightly less than that of silk.

The only parameters in our simple elastic structural model in this study are the stiffness of the backbone and H bond, which are obtained directly from atomistic simulation and modeling, and the current analysis is based on parameters at room temperature and in a water environment. Nevertheless, our model can, in principle, be used to predict differences as a result of variations of these parameters, including the effect of different external factors that include changes in the *p*H value, the temperature, or the solvent composition [16,31,35], as long as the modified backbone and H-bond stiffnesses are obtained from either simulation or experiment.

IV. CONCLUSION

Our results provide insight into the size of region in which H-bond deformation is cooperative for both beta-strands and beta-sheet nanocrystals, which is important to predict the ultimate tensile strength and mechanism. We find that the external force deforms H bonds significantly only within a relatively small region that is of the approximate size of several H bonds. The most important conclusion from this study is that in order to ensure maximum usage of H bonds, the size of clusters of H bonds must be confined to extremely small values to match the size of the cooperative deformation. This insight is important in designing the nanoscale structure of polymer matrix materials to achieve optimized mechanical properties despite weak building blocks [3].

Moreover, a comparison with the size of H-bond clusters found in biology revealed an excellent agreement with the cluster sizes predicted by our analysis. This has potentially profound implications as it suggests that perhaps the confinement of H bonds into nanoscale elements is a universal biological design paradigm that turns weakness to strength and thereby overcomes the mechanical limitations of H bonds in creating strong and tough materials.

Our model could be directly applied to other protein and polymer materials and could aid in the design of novel biologically inspired materials. Applications could, in principle, also include strong bonds such as covalent or ionic bonds and focus on other weak bonds such van der Waals forces or dipole-dipole interactions.

ACKNOWLEDGMENTS

Support from AFOSR (Grant No. FA9550081-0321), ARO (Grant No. W911NF-10-0127), and ONR (Grants No. N000141010562 and No. N000140810844) is acknowledged.

[1] Z. Z. Shao and F. Vollrath, Nature (London) **418**, 741 (2002).
[2] C. Vepari and D. L. Kaplan, Prog. Polym. Sci. **32**, 991 (2007).
[3] M. J. Buehler and Y. C. Yung, Nature Mater. **8**, 175 (2009).
[4] N. Huebsch and D. J. Mooney, Nature (London) **462**, 426 (2009).
[5] M. Denny, J. Exp. Biol. **65**, 483 (1976).
[6] P. A. Guerette, D. G. Ginzinger, B. H. F. Weber, and J. M. Gosline, Science **272**, 112 (1996).
[7] T. Lefevre, M. E. Rousseau, and M. Pezolet, Biophys. J. **92**, 2885 (2007).
[8] J. D. van Beek, S. Hess, F. Vollrath, and B. H. Meier, Proc. Natl. Acad. Sci. U.S.A. **99**, 10266 (2002).
[9] S. Keten and M. J. Buehler, Appl. Phys. Lett. **96**, 153701 2010.
[10] S. Keten and M. J. Buehler, J. R. Soc. Interface (2010), doi: 10.1098/rsif.2010.0149
[11] S. M. Lee, E. Pippel, U. Gosele, C. Dresbach, Y. Qin, C. V. Chandran, T. Brauniger, G. Hause, and M. Knez, Science **324**, 488 (2009).
[12] F. Vollrath and D. Porter, Soft Matter **2**, 377 (2006).

[13] N. Du, X. Y. Liu, J. Narayanan, L. Li, M. L. Lim, and D. Li, Biophys. J. **91**, 4528 (2006).
[14] S. Keten, Z. P. Xu, B. Ihle, and M. J. Buehler, Nature Mater. **9**, 359 (2010).
[15] A. Nova, S. Keten, N. M. Pugno, A. Redaelli, and M. J. Buehler, Nano Lett. **10**, 2626 (2010).
[16] Z. Qin and M. J. Buehler, Phys. Rev. Lett. **104**, 198304, 2010.
[17] M. J. Buehler, *Atomistic Modeling of Materials Failure* (Springer, New York, 2008).
[18] S. L. Mayo, B. D. Olafson, and W. A. Goddard, J. Phys. Chem. **94**, 8897 (1990).
[19] B. R. Brooks, R. E. Bruccoleri, B. D. Olafson, D. J. States, S. Swaminathan, and M. Karplus, J. Comput. Chem. **4**, 187 (1983).
[20] C.-I. Branden and J. Tooze, *Introduction to Protein Structure*, 2nd ed. (Garland Publishing, New York, 1999), 410.
[21] S. J. Lombardi and D. L. Kaplan, J. Arachnol. **18**, 297 (1990).
[22] T. Lazaridis and M. Karplus, Proteins: Struct., Funct., Genet. **35**, 133 (1999).
[23] T. Lazaridis and M. Karplus, Science **278**, 1928 (1997).
[24] H. Grubmuller, Phys. Rev. E **52**, 2893 (1995).
[25] M. M. Tirion, Phys. Rev. Lett. **77**, 1905 (1996).
[26] S. Keten and M. J. Buehler, Phys. Rev. Lett. **100**, 198301 (2008).
[27] M. Sotomayor and K. Schulten, Science **316**, 1144 (2007).
[28] S. Keten and M. J. Buehler, Nano Lett. **8**, 743 (2008).
[29] S. A. Fossey, G. Nemethy, K. D. Gibson, and H. A. Scheraga, Biopolymers **31**, 1529 (1991).
[30] S. Penel, R. G. Morrison, P. D. Dobson, R. J. Mortishire-Smith, and A. J. Doig, Protein Eng. **16**, 957 (2003).
[31] T. Ackbarow, X. Chen, S. Keten, and M. J. Buehler, Proc. Natl. Acad. Sci. U.S.A. **104**, 16410 (2007).
[32] K. Tsemekhman, L. Goldschmidt, D. Eisenberg, and D. Baker, Protein Sci. **16**, 761 (2007).
[33] E. Oroudjev, J. Soares, S. Arcdiacono, J. B. Thompson, S. A. Fossey, and H. G. Hansma, Proc. Natl. Acad. Sci. U.S.A. **99**, 6460 (2002).
[34] *Steel Construction Manual*, 13th ed. (American Institute of Steel Construction, Chicago, IL, 2005), Vol. 1.
[35] Z. Qin, L. Kreplak, and M. J. Buehler, Nanotechnology **20**, 425101 (2009).